Environmental Geotechnics

Geothermal energy in loess
Bidarmaghz, Makasis, Narsilio, Francisca and Carro Pérez

Environmental Geotechnics
http://dx.doi.org/10.1680/jenge.15.00025
Paper 15.00025
Received 07/05/2015; accepted 19/11/2015
Keywords: geothermal/numerical modelling/piles/temperature effects

ice Institution of Civil Engineers
publishing

Geothermal energy in loess

1 **Asal Bidarmaghz** PhD, MSc, BSc
Department of Infrastructure Engineering, The University of Melbourne, Parkville, Australia

2 **Nikolas Makasis** MSc, MEng
Department of Infrastructure Engineering, The University of Melbourne, Parkville, Australia

3 **Guillermo A. Narsilio** PhD, MSc, MSc, CEng
Australian Research Council Future Fellow and Senior Lecturer, Department of Infrastructure Engineering, The University of Melbourne, Parkville, Australia (corresponding author: narsilio@unimelb.edu.au)

4 **Franco M. Francisca** PhD, CEng
Institute for Advanced Studies in Engineering and Technology (IDIT), Universidad Nacional de Córdoba and Consejo Nacional de Investigaciones Científicas y Técnicas (Conicet), Córdoba, Argentina

5 **Magalí E. Carro Pérez** PhD, MSc, CEng
IDIT, Universidad Nacional de Córdoba and Conicet, Córdoba, Argentina

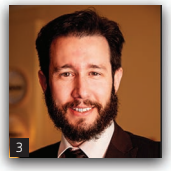

Ground-source heat pump (GSHP) systems efficiently heat and cool buildings by using sustainable geothermal energy accessed by way of ground heat exchangers (GHEs). Loess covers vast parts of the world, about 10% of the landmass; therefore, the use of piles or 'micropiles' is extensive in these areas, particularly where the thickness of loessic soils is significant. These deep foundations have the potential to be used as 'energy piles' in GSHP systems, with a minimal additional cost. This paper presents a case study of a representative real building in Córdoba, Argentina, where foundations are also used as GHEs. The thermal properties of local soils were experimentally measured and used in recently developed detailed state-of-the-art finite-element models. Results from the realistic simulations show that the partial substitution of electrical heating and cooling systems with geothermal systems could significantly reduce energy consumption and the size of associated infrastructure, despite the relatively low thermal conductivity of local loess. Moreover, the effects of surface air temperature fluctuations, which are routinely ignored in GHE design, are accounted for in these simulations. This case study shows the potential of GSHP technology in loessic environments and gives incentives to engineers to start considering the technology in their designs and practices.

Notation

A	inner cross-sectional area of a pipe: m^2
A_s	earth surface temperature annual swing above and below the average ground temperature: °C
$C_{p,m}$	specific heat capacity of solid material: J/(kg K)
$C_{p,w}$	specific heat capacity of carrier fluid: J/(kg K)
d_h	hydraulic diameter of pipe: m
f_D	Darcy friction factor
k_v	vegetation coefficient
p	pressure: Pa
Q_{wall}	external heat exchange rate through pipe walls: W/m
T	fluid temperature: °C
$T(z, t)$	depth and time-varying temperature: °C
$T_{far\text{-}field}$	undisturbed ground temperature: °C
T_g	annual average ground temperature: °C
T_{inlet}	average inlet pipe temperature: °C
T_m	temperature of solid material: °C
$T_{m,pipe\ wall}$	temperature of solid material at the pipe outer wall: °C
T_{outlet}	average outlet pipe temperature: °C
t	time: s (Equations 1–4), d (Equation 5)
t_0	number of days after 1 January to the minimum earth surface temperature: d
$\boldsymbol{v}$	fluid velocity field: m/s
x, y, z	Cartesian coordinates, with z denoting depth: m
z	depth below the ground surface: m
α	soil thermal diffusivity: $\times 10^{-2}$ cm^2/s
λ_m	thermal conductivity of solid material: W/(m K)
λ_w	thermal conductivity of the carrier fluid: W/(m K)
ρ_m	density of solid material: kg/m^3
ρ_w	density of carrier fluid: kg/m^3

Introduction: ground-source heat pump systems and loess deposits

Ground-source heat pump (GSHP) systems efficiently heat and cool buildings by using sustainable geothermal energy accessed by way of ground heat exchangers (GHEs). In closed-loop systems, GHEs comprise high-density polyethylene (HDPE) pipes embedded in specifically drilled boreholes or trenches or even

built into foundations, all within a few tens of metres of the surface (Figure 1). GSHP systems operate at a coefficient of performance of about 4 throughout the year, basically delivering 4 kW of heating or cooling for every kilowatt input into running the heat pumps (Amatya *et al*., 2012; Brandl, 2006; Johnston *et al*., 2011; Preene and Powrie, 2009).

Loess is an unstable soil that develops collapse due to water content and/or load increases. Loessial soils are loosely cemented aeolian sediments composed mainly by fine sand, silt and clay particles that accumulate when deposited by wind (*primary loess*) and sometimes particles are retransported by either water or snow (*secondary loess*). In both cases, particles are frequently cemented by either precipitated calcium carbonate or silicates (Francisca, 2007; Moll and Rocca, 1991; Rocca *et al*., 2006). Loess covers vast parts of the world, about 10% of the landmass, and is encountered across New Zealand, from Western Europe to China (including Russia), across North America and in regions across South America (Quintana Crespo, 2005; Rocca *et al*., 2006; Zárate, 2003). In particular, loess deposits cover large areas of Córdoba, Argentina, and are tens of metres thick.

To support the structures constructed on this type of soil, the use of piles (>300 mm diameter) for multistorey buildings or 'micropiles' (<300 mm diameter) for lighter residential buildings is quite extensive. These foundations, which are already required for construction purposes, can serve a dual purpose both as foundations and as GHEs (i.e. energy piles). No extra costs (except the minor pipe costs) for drilling and installation are added as the already built structural piles are used as GHEs. However, there are virtually no studies conducted on the feasibility and design of geothermal systems in loessial soils and there is a missed opportunity in current practice to use deep foundations as structural elements and as GHEs when dealing with loessial sites. The GSHP alternative becomes even more attractive in areas where natural gas infrastructure is not available and only expensive liquefied petroleum gas or wood is used for heating. GSHP systems can significantly reduce the use of these fuels in these (predominantly rural) areas and at the same time can provide an alternative clean energy for conditioning of buildings.

To exemplify the benefits of GSHP systems in loess deposits and highlight potential issues, this paper presents a numerical case study of a representative real building in Córdoba, where foundations are also used as GHEs. While this study focuses on the thermal performance of energy piles, the effect of cyclical heating and cooling on the structural and geotechnical strength of piles is a necessary aspect to also consider in geothermal projects; however, this latter aspect is beyond the scope of this work. Nevertheless, it is important to note that in the case of loess, structural concerns may arise from rupture or leakage of HDPE pipes and water filtration into this collapsible soil. It is therefore crucial to ensure a high standard in quality assurance and quality control of the thermo-fused pipe joints. This is routinely achieved by way of visual inspections and subsequent pressure tests of the U loops before and after casting and during commissioning of the GSHP systems, as outlined in various International Ground Source Heat Pump Association guidelines (Oklahoma State University, 2009).

Main characteristics of loess

Loess is a quaternary sediment composed mainly of fine particles that form an open microstructure. Therefore, this soil is characterised by an internal structure that controls the thermo-hydro-mechanical behaviour of loessial formations. Loess is an unstable soil that develops collapse due to water or internal pressure increases. This produces significant settlements that affect civil infrastructure and structures that suffer significant distortions (Rocca *et al*., 2006). Loessial soils cover approximately 10% of the continents, including North America, Europe, Asia and South America (Rinaldi *et al*., 2007). The most significant loess formations are found in Argentina (Iriondo, 1997; Zárate, 2003), the Czech Republic (Marschalko *et al*., 2013), China (Kukla and An, 1989), Russia (Little *et al*., 2002), Spain (Günster *et al*.,

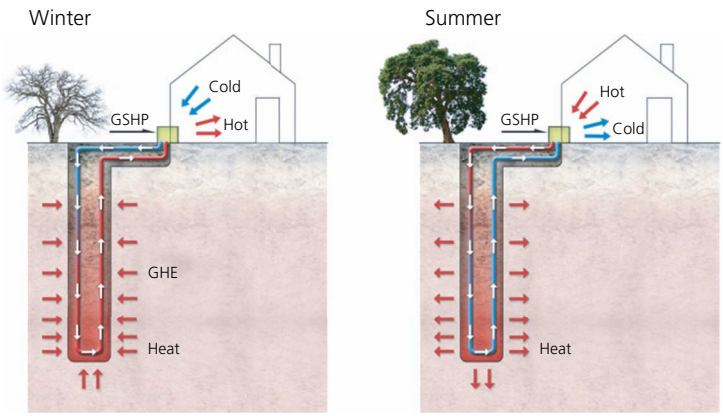

Figure 1. Schematic diagram of a GSHP system in heating (winter) and cooling (summer) modes (Note: not to scale)

2001) and the USA (Leighton and Willman, 1950). All these formations are characterised by a macroporous structure with very high void ratio (typically from 0·9 to 1·25), predominantly fine granulometry mainly composed of silt- and clay-size particles and poorly accommodated structure. As a consequence, loess collapses when water and pressure increases. This phenomenon produces significant damage to buildings constructed on shallow foundations (Rocca, 1985). Different loessial soils can be found depending on whether they suffered changes in the original structure. Primary loesses are those that preserve the original structure generated when they were deposited, while secondary loesses arise when particles of primary loess are transported by any other action such as gravity, water or snow.

Loess formations cover approximately 35% of Argentina (Terzariol, 2009) with a thickness that varies from 10 m to more than 60 m, thus making these formations a good candidate to investigate GSHP system applicability in loess. In general, the mineralogy of Argentinean loess is characterised by an abundance of plagioclase (20–60%), relatively little quartz (20–30%) and a significant percentage of volcanic glass (15–30%), and calcium carbonate (2–10%) (Teruggi, 1957). The Argentinean loess also has significant fraction of volcanic glass as a major component of the silt and sand fractions in comparison with other loess formations around the world (Kostić and Protić, 2000; Kröhling and Iriondo, 1999).

The open structure, large void ratio and mineralogy of loess control the heat flow in these formations. In addition, tillage systems and compaction influence soil thermal properties as well as volumetric water content (Guan *et al*., 2009; Usowicz *et al*., 1996). There is limited literature about the thermal characteristics of loess. Nevertheless, Table 1 summarises the most significant thermal properties of different loessial soils around the world. The most frequent thermal conductivity of Argentinean loess is close to 0·65 W/(m K) and tends to increase with the water content and bulk density of the soil (Dec *et al*., 2009; Gogół *et al*., 1973; Guan *et al*., 2009; He *et al*., 2000; Johnson and Lorenz, 2000; Kodešová *et al*., 2013; Narsilio *et al*., 2015; Usowicz *et al*., 1996; Wang *et al*., 2007; Zuo *et al*., 2011).

Site description and thermal characterisation

The case study, a residential building, is located 2 km west of Córdoba City (Argentina) and consists of a typical residential two-storey building with a footprint of approximately 85 m^2 in a 475 m^2 block of land (17·6 m × 27 m) (Figure 2(a)). The geological formation corresponds to a wind plain aggradation mid-Pleistocene to early Holocene. This domain is characterised in the field of Córdoba City and its periphery, on both sides of the valley of the Suquía River, by a gently undulating plane of sedimentary cover – loessoide silt with a regional tilt to the east of the order of 0·5%.

Site/location	Thermal conductivity: W/(m K)	Volumetric heat capacity: MJ/(m^3 K)	Specific heat capacity[a]: J/(kg K)	Bulk density: kg/m^3	Volumetric moisture content: %	Source
Poland	0·5–1·75			1230–1820	0·0–20·0	Gogól *et al*. (1973)
Felin, Poland	0·47–1·98	1·39–2·42		1320–1410	10·5–24·8	Usowicz *et al*. (1996)
Fangshan County, China	0·352, 0·344, 0·311	1·44, 1·39, 1·27		—	—	He *et al*. (2000)
Alaska, USA:						
CRREL Permafrost Tunnel	0·07–0·18			700–1000	5·7–8·0	Johnson and Lorenz (2000)
Birch Hill field sample	0·15	—		1160	1·9	
Chena Spur Road sample	0·73, 0·8			1350, 1360	3·8, 6·5	
China	0·29–1·65	1·497–2·95		1050–1650	0·5–43·5	Wang *et al*. (2007)
Loess Plateau, China	0·4–1·5	0·01–2·5		—	5·5–16·0	Guan *et al*. (2009)
Northern Germany	0·91–1·08	2·00–2·90		1470–1530	18·0–42·5	Dec *et al*. (2009)
Gansu, China	1·0	—		1200–1240	—	Zuo *et al*. (2011)
Suchdol, Czech Republic	0·25–1·5	1·1–3·1		1310	—	Kodešová *et al*. (2013)
Córdoba, Argentina	0·36–0·88	—		1200–1400	13·5–33·0	Narsilio *et al*. (2015)

[a] Estimated based on the reported data.
CRREL: Cold Regions Research and Engineering Laboratory.

Table 1. Loess thermal conductivity ranges in different places around the world

The formation consists of four distinguishable layers (Figure 2(b)): non-plastic silt with some organic matter (z = 0–0·3 m below ground surface); collapsible non-plastic silt with some clay and sand (z = 0·3–9·5 m) (primary loess); low-plasticity silt with sand (z = 9·5–13 m) and a sand with silt and gravel layer (z > 13 m).

The water table was not found within 14 m below the ground surface at the time of the geotechnical site investigation, which was conducted during the dry season (winter). However, the groundwater table in this region is known to be located deeper than 20 m. In the loess layer, the natural water content was found to be about 17% and the dry density was about 1400 kg/m^3 (thus, a total density of the order of 1600 kg/m^3). The water content profile measured up to 5 m in depth is shown in Figure 2(b) and for modelling purposes ('Numerical modelling' section), it is assumed constant throughout the year, with the above value taken as representative.

The foundations of this case study involve a total of 13 bored piles, 9·5 m deep, with nine piles of 0·4 m diameter and four (central) piles of 0·6 m diameter. Due to the relatively short length of the piles, the groundwater table is expected to be deeper than the depth of the piles throughout the year.

The thermal needle probe method was used for the determination of thermal conductivity of 'typical' loessial silts from Córdoba following ASTM recommendations (ASTM, 2008). Figure 3 summarises the measured thermal conductivities for a range of dry densities and water contents, resulting between 0·36 and 0·88 W/(m K).

Numerical modelling

The aforementioned information is used in detailed finite-element simulations of the GHE field corresponding to the building foundations using a recently developed state-of-the-art model, details of which can be found in Bidarmaghz (2014) and Bidarmaghz *et al.* (2016). The model can account for the local geology, surface thermal recharge and the local weather for a more realistic representation of GHEs' thermal behaviour. An overview of the model and the geometry and initial and boundary conditions of the case study follows.

Governing equations

A three-dimensional (3D) numerical model based on fundamental principles has been developed and implemented using finite-element methods. The governing equations for fluid flow and heat transfer are coupled numerically within the finite-element package Comsol Multiphysics to evaluate the thermal performance of GHEs. Although important, the mechanical behaviour of the energy piles is outside the scope of this work and this study focuses on only the thermal responses of energy piles under realistic heating and cooling cycles.

Heat transfer around and in the GHEs is modelled primarily by conduction and convection. Heat conduction occurs in the soil, GHE backfilling material (concrete) and HDPE pipe wall and partially in the carrier fluid (water). Heat convection dominates in the carrier fluid circulating in the pipes as there is no groundwater flow in the ground (the groundwater table was not found at the site). In this modelling, the fluid flow and heat

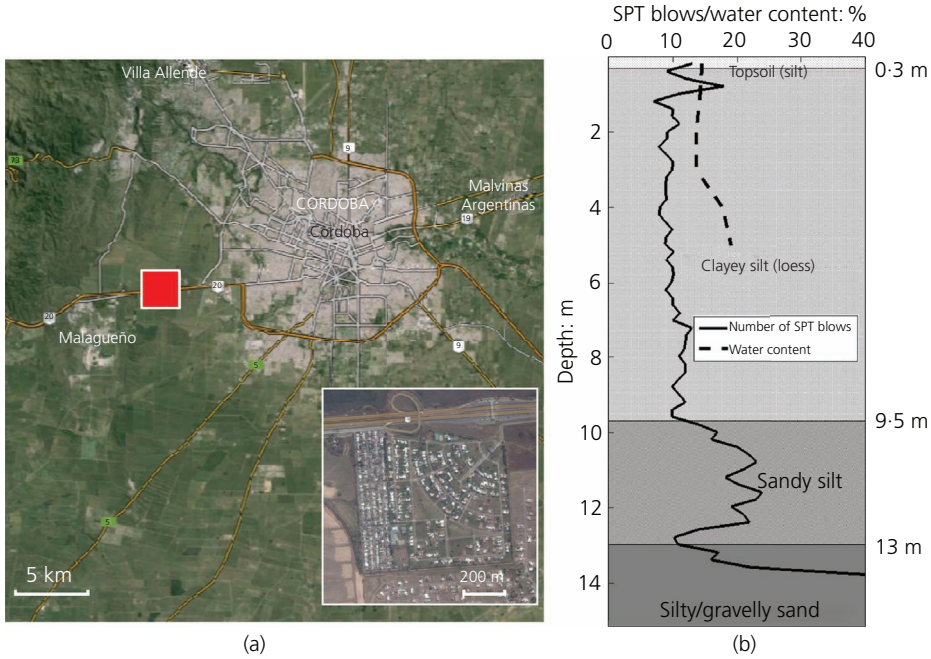

Figure 2. (a) Site location; (b) representative soil profile, water content and SPT profile within the site. Data courtesy of GEoS and Profundar

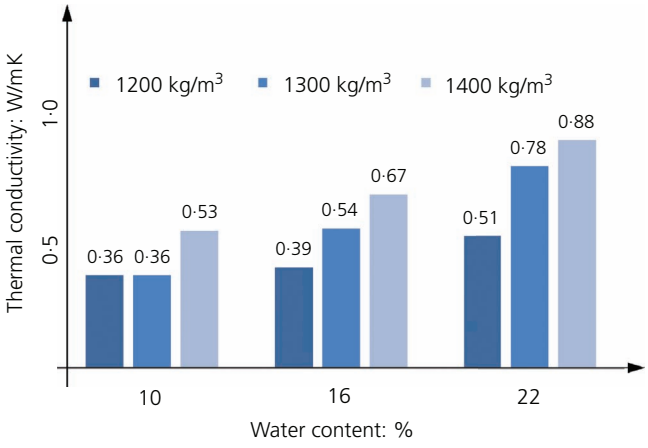

Figure 3. Measured Córdoba loess thermal conductivity for a range of water contents and dry densities

transfer in the carrier fluid are coupled to the heat transfer in the pipes, the GHEs and the surrounding soil.

The fluid-flow regime in the long pipes is considered as fully developed (e.g. the entrance length of a typical 25 mm round pipe is only about 0·5 m); thus, the fluid flow and the heat transfer in the fluid are simulated using one-dimensional (1D) elements and are coupled to the 3D heat transfer in the GHEs and the surrounding soil.

To model the 1D fluid flow inside the pipes, the continuity and momentum equations for incompressible fluid are used as follows (Barnard *et al.*, 1966).

1. $$\nabla(A\rho_{\mathrm{w}}\boldsymbol{v}) = 0$$

2. $$\rho_{\mathrm{w}}\left(\frac{\partial \boldsymbol{v}}{\partial t}\right) = -\nabla p - f_{\mathrm{D}}\frac{\rho_{\mathrm{w}}}{2d_{\mathrm{h}}}|\boldsymbol{v}|\boldsymbol{v}$$

where A is the inner cross-section of the HDPE pipe, ρ_{w} is the carrier fluid density, $\boldsymbol{v}$ represents the fluid velocity field, t shows the time, p is the pressure, f_{D} represents the Darcy friction factor and d_{h} is the hydraulic diameter of the pipe. The energy equation for the fluid flow to describe the convective–conductive heat transfer for an incompressible fluid is (Lurie, 2008)

3. $$\rho_{\mathrm{w}}AC_{\mathrm{p,w}}\frac{\partial T}{\partial t} + \rho_{\mathrm{w}}AC_{\mathrm{p,w}}\boldsymbol{v}\nabla T = \nabla(A\lambda_{\mathrm{w}}\nabla T) + f_{\mathrm{D}}\frac{\rho_{\mathrm{w}}A}{2d_{\mathrm{h}}}|\boldsymbol{v}|\boldsymbol{v}^2 + Q_{\mathrm{wall}}$$

where $C_{\mathrm{p,w}}$ is the specific heat capacity of the fluid, λ_{w} represents the thermal conductivity of the fluid and Q_{wall} is the external heat exchange rate through the pipe wall. The above equations are solved for pressure p, velocity field $\boldsymbol{v}$ and temperature field T in the carrier fluid and are coupled to the temperature field T_{m} obtained from the conductive heat transfer equations solved for the soil, the GHEs and the pipes (Equation 4). The coupling arises from the Q_{wall} term in Equation 3, as Q_{wall} is directly proportional to the temperature inside the HDPE pipe T and the temperature on the outer wall of the HDPE pipe $T_{\mathrm{m,pipe\ wall}}$. It should be noted that heat transfer in the soil, the GHEs and the pipe wall is purely conductive due to the absence of ground water flow.

4. $$\rho_{\mathrm{m}}C_{\mathrm{p,m}}\frac{\partial T_{\mathrm{m}}}{\partial t} = \nabla(\lambda_{\mathrm{m}}\nabla T_{\mathrm{m}})$$

where ρ_{m} represents the solid material density and $C_{\mathrm{p,m}}$ and λ_{m} are the specific heat capacity and the thermal conductivity of the given solid material (soil, concrete, and HDPE) respectively. This model, completed with appropriate initial and boundary conditions, has recently been validated against available analytical solutions, and full-scale experimental data (Bidarmaghz, 2014; Bidarmaghz *et al.*, 2016). The model is capable of accurately predicting heat transfer between the ground and the GHEs in both laminar and turbulent regimes and homogeneous and heterogeneous soil profiles and flexible in exploring a number of different pipe placement configurations in steady-state and transient conditions.

Case study: geometry, initial and boundary conditions

The finite-element model and the key initial and boundary conditions, together with the GHEs' (piles) configuration, are shown in Figure 4. The 13 GHEs are spaced between ~2 and 4·4 m. Only the four piles in the middle row are 0·6 m in diameter, allowing the insertion of three HDPE U loops, whose spacing between inlet and outlet pipes is 0·16 m (a detail is shown in the figure as well). The remaining nine piles can accommodate only two of these U loops, given their reduced diameter of 0·4 m. It should be noted that these GHEs are bored piles; therefore, full contact between the concrete and the soil is expected and considered in these simulations. However, isolated air pockets (incomplete concreting or imperfections in the pile) may reduce GHE (structural and thermal) efficiency. The size of the ground domain in the numerical model(s) is based on a sensitivity analysis conducted on the distance between the outer GHEs and the 'external' boundaries of the ground, such that the far-field boundaries are far enough from the GHEs in all models to avoid artificial edge effects (minimum distance of 8 m).

The parameters used in all numerical models are shown in Table 2. The initial and far-field ground temperature $T_{\mathrm{far\text{-}field}}$ varies with depth z and time t of the year; these variations derive from the surface air fluctuations throughout the year, particularly in the upper few metres of the soil (i.e. about 4 m in Córdoba, Argentina). However, the average soil temperature deeper than about 4 m tends to be very close to the mean ambient temperature throughout the year at this location (i.e. 18°C).

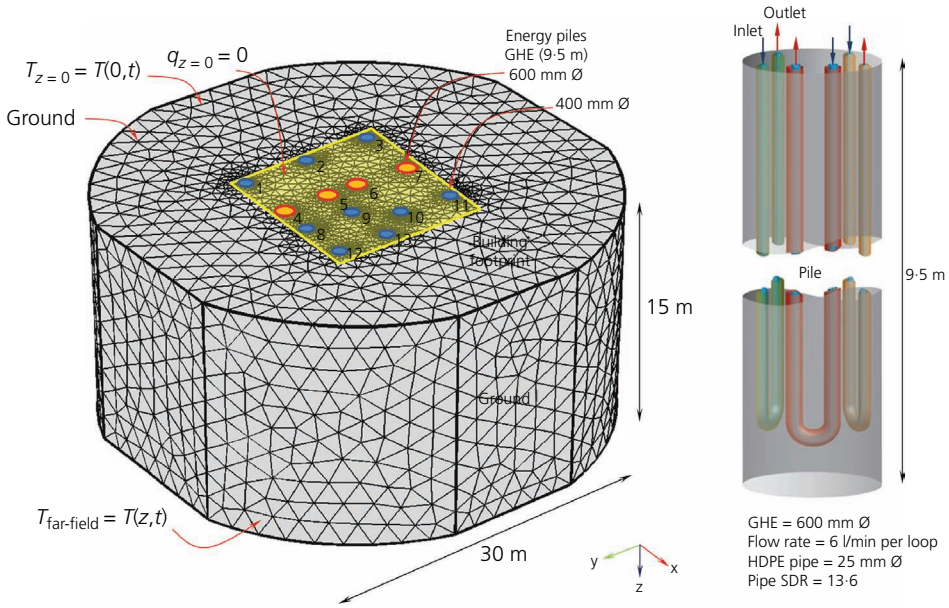

Figure 4. (a) Finite-element model used in the simulations, with soil limits far enough to minimise artificial boundary effects and the building footprint; (b) a detail of a 0·6 m energy pile

Thus, some heat is exchanged between the air and the ground (surface thermal recharge/discharge) and it is accounted for in additional simulations following Baggs's adjusted empirical formulations (Baggs *et al.*, 1991).

$$T(z,t) = T_g + 1{\cdot}07\,k_v A_s \exp\left[-0{\cdot}0031552z\left(\frac{1}{\alpha}\right)^{0{\cdot}5}\right] \cos\left\{\frac{2\pi}{365}\left[(t - t_0 - 0{\cdot}18335z)\left(\frac{1}{\alpha}\right)^{0{\cdot}5}\right]\right\} \quad (5)$$

where $T(z,t)$ is the ground temperature at depth of z metres after t days from 1 January taken as $T_{far\text{-}field}$ and as initial condition, T_g is the average annual ground temperature (18°C in Córdoba, Argentina), k_v is the vegetation coefficient taken equal to 0·50 in this study (according to Baggs *et al.*, 1991, for ground in full sun $k_v = 1$ and for a long grass-covered area $k_v = 0{\cdot}25$), A_s is the earth surface temperature annual swing above and below the average ground temperature (14°C), t_0 represents the number of days after 1 January to the minimum earth surface temperature (238 d in Cordoba) and α stands for the soil thermal diffusivity ($0{\cdot}3645 \times 10^{-2}$ cm^2/s).

For simplicity, the annual peak building thermal load was estimated based on rules of thumb for typical gated community residencies in Córdoba (heating = 0·035 kW/m^3 or 30 kcal/(h m^3); cooling = 0·058 kW/m^3 or 50 kcal/(h m^3)) rather than detailed energy balance calculations. This case study comprises a total of 160 m^2 covered area, of which 20 m^2 is for a double garage that does not need conditioning. Thus, for 2·6 m high ceilings, the peak heating and cooling demands result in approximately 12·7 and 21·1 kW respectively.

Results and discussions

There are a number of design strategies that could be implemented when deciding on a residential GSHP system, including aiming to provide 100% of the heating and cooling required or to combine geothermal with auxiliary systems (i.e. designing a hybrid system) in all cases avoiding ground freezing that could lead to ground heave or damage to concrete in the pile (Loveridge and Powrie, 2014). Perhaps the first question to be answered is what the geothermal installed capacity of this residential building would be if all 13 of its piles were used as GHEs. Figure 5(a) shows the total building heating and cooling demand distribution throughout a year, based on the peak demands (12·7 and 21·1 kW; 'Case study: geometry, initian and boundary conditions' section) and the air temperature recorded in 2014.

The newly developed numerical model revealed that the 13 piles are unable to satisfy 100% of both heating and cooling thermal demands of the building. Thus, one alternative is to consider hybrid systems: the GSHP system covers part of the demand and the auxiliary systems (e.g. smaller gas heater(s), smaller air conditioner unit(s) and thermal solar panels and busters) are either used to top up the supply of heating or cooling (case 1) or just turned on when this base demand exceeds the geothermal capacity

Material	Thermal conductivity: W/(m K)	Specific heat capacity: J/(kg K)	Density: kg/m^3	$T_{far\text{-}field}$: °C	Diameter: m	Spacing: m
Loess (soil)	0·700	1200	1600	$T(z, t)$	—	—
Concrete (piles)	2·100	850	2350	—	0·4, 0·6	2–4·4
HDPE (pipe)	0·400			—	0·025	0·16
Water (fluid)	0·582	4180	1000	—	—	—

Table 2. Summary of the key input parameters used in the numerical models

(case 2). Case 1 implies that the auxiliary system is running all the time concurrently with the GSHP, while case 2, only a number of days each year.

As presented in Figure 5(a), case 1 indicates that the GSHP system is designed to provide half and one third of total heating and cooling demand of the house respectively, with an auxiliary system being used 246 d in heating mode and 118 d in cooling mode. The geothermal system satisfies up to 7 kW of the peak heating and cooling demand of the house. In the other case (case 2), the GSHP system also has the same 7 kW peak capacity; however, due to the different thermal load distribution, the geothermal system is aimed at satisfying almost all heating and more than half of the cooling demand of the house with significantly fewer days of auxiliary systems being used.

To highlight how the GHE field will perform and react to the defined thermal loads, the modelled average fluid temperature variations (i.e. $(T_{inlet} + T_{outlet})/2$) in the most demanded GHE (pile 5; Figure 4) obtained from 20-year numerical simulations are presented in Figure 5(b). It is observed that satisfying case 1's thermal load distribution results in a reasonable temperature range (3·1–44·3°C) compatible with most commercially available heat pumps. On the other hand, case 2 results in a fluid temperature drop to a minimum of −2·2°C in cold seasons (which is acceptable with an antifreeze solution used as carrier fluid instead of plain water) and a rise to the maximum of 56·5°C in warm seasons. This maximum fluid temperature for case 2 is higher than typical GSHP recommended temperature for water entering the heat pump (EWT). It follows that this GHE field, using the structural piles, is not capable of delivering the more desirable thermal load defined for case 2. Thus, this article focuses on case 1 from here on.

Figure 6 shows the temperature field at middepth of the energy piles (about 5 m below ground surface) (year 10). The figure shows that freezing is avoided in the GHE field for case 1, with no point within the soil or the energy piles reaching less than 4·8°C, even during the coolest seasons when the GHEs extract more of the thermal heat from the ground. Therefore, potential structural problems due to concrete freezing and/or soil heaving are circumvented.

From these results, it follows that even though the low thermal conductivity of loess (0·7 W/(m K)) and relatively shallow GHEs (~10 m) affect the thermal efficiency of the GSHP systems, the incorporation of a GSHP system into the essential 13 structural piles (described in 'Site description and thermal characterisation' section) leads to about 30% savings in conventional energy usage (e.g. electricity or fossil fuels) and in energy bills, with the GSHP satisfying at least 54% of the heating needs and 33% of the cooling needs. Although this GHE field cannot provide 100% of the required heating and cooling demand, it can be used to provide part of the building thermal demand with little additional capital cost.

To increase the capacity of the GSHP system conditioning the case study building, another alternative would be drilling additional GHEs outside the footprint of the house in the available block of land. Increasing the number of GHEs may lead to some extra drilling costs; however, it may also have significant influence on further reducing running energy costs. Therefore, 12 9·5 m long GHEs are added to the original GHE-field, bringing the total number to 25. These additional GHEs do not serve any structural purpose. Surface thermal recharge is also accounted for. Figure 7 shows a schematic diagram of the GHEs and their locations within the available block of land with 12 GHEs being added to the original GHE field. The extra GHEs are of 0·6 m diameter, contain three U loops, and are of the same depth as the rest of the GHE field (9·5 m long GHEs).

The building thermal load applied as one of the boundary conditions on the model is shown in Figure 8 with 12·7 kW of peak heating and cooling demand now aimed to be satisfied (instead of 7 kW).

The average fluid temperature obtained from one of the most thermally influenced GHEs (pile 5) is shown in Figure 9. Satisfying a peak load of 12·7 kW heating and cooling leads to the fluid temperature varying within a reasonable range (i.e. maximum of 37·2°C and minimum of 6·8°C). The extra 12 GHEs in the GHE field results in 100% of the heating demand and 60·2% of the cooling demand being provided by the GSHP system. A significant improvement in heating and cooling capability of the system is obtained in comparison to the cases investigated in cases

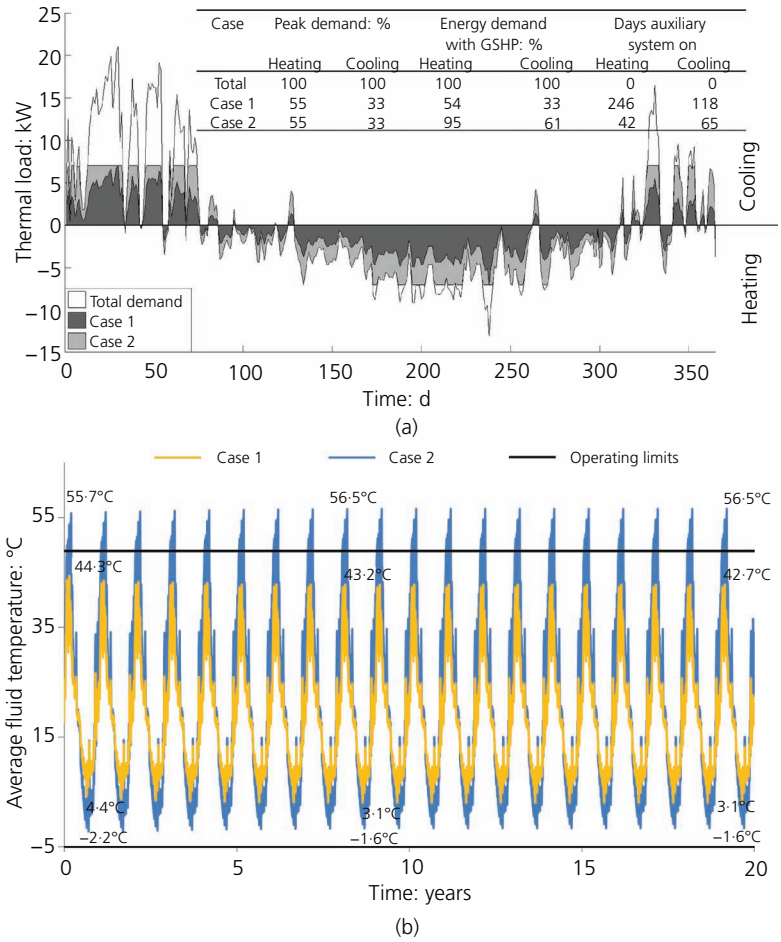

Figure 5. (a) Thermal load distributions throughout a year and (b) GHE response over a 20-year period (including typical GSHP operating EWT range)

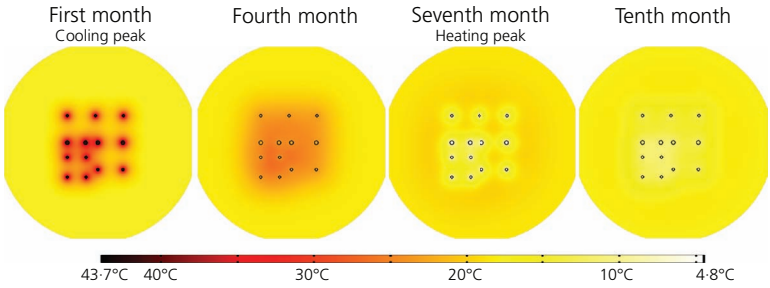

Figure 6. Temperature field in the 13 piles and surrounding soil at 5 m below surface (year 10)

1 and 2. Moreover, the even smaller (and cheaper) auxiliary conditioning system is required for 118 d per year and only in cooling mode. The savings in the installation of auxiliary systems and on running costs would determine the economic feasibility of the additional drilling costs.

GSHP system designers and potential users of these systems should be aware that inadequate designs (or drastic changes in the thermal load patterns) may lead to more pronounced overheating or overcooling of the soil in the medium term until reaching a periodic thermal equilibrium. This change or drift in the overall

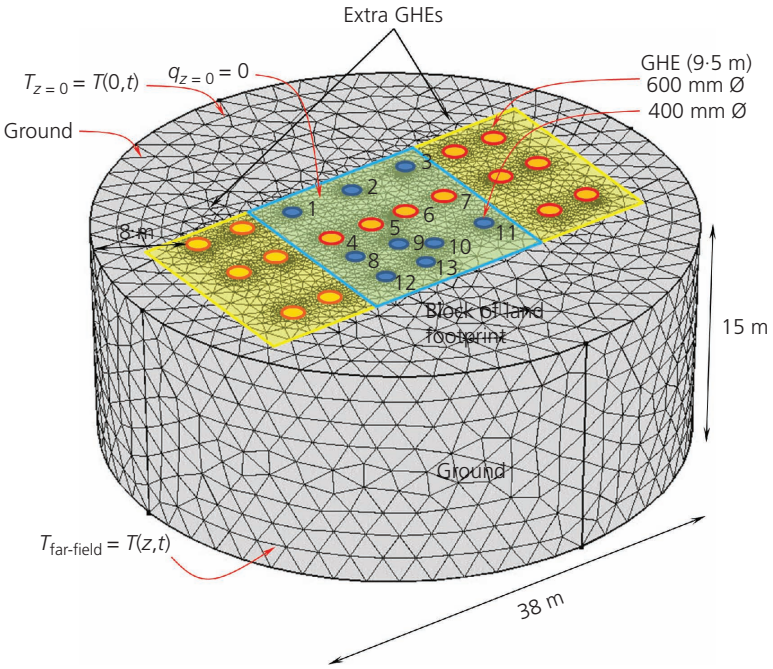

Figure 7. Schematic diagram of the expanded GHE field and location of the GHEs within the block of land

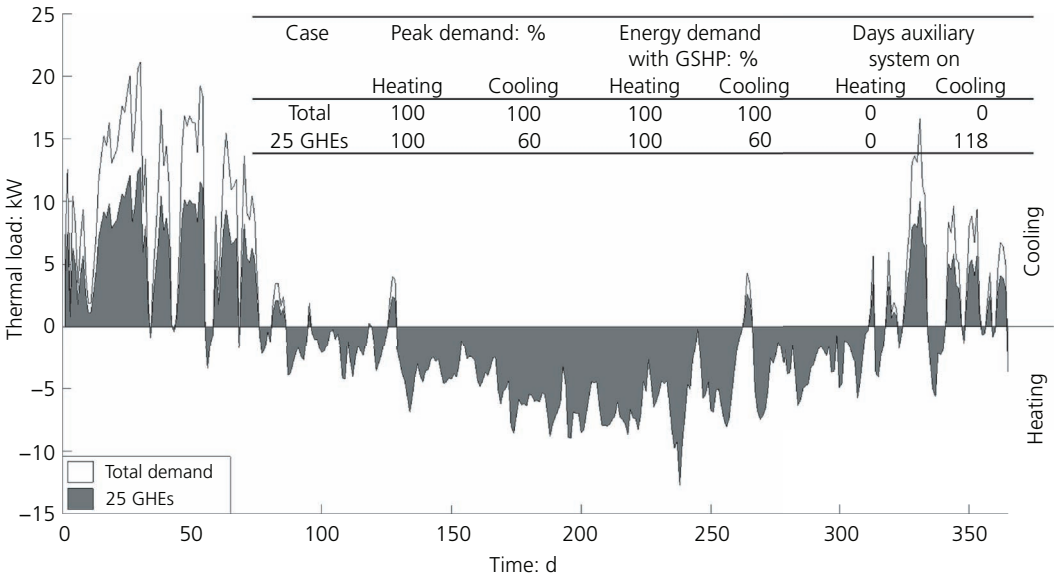

Figure 8. Building thermal load applied on the model with extended number of GHEs (25 GHEs)

ground temperature from year to year inevitably influences the efficiency of the system over time, thus affecting the running costs and saving levels of the GSHP systems during their life span.

Loessial soils in Córdoba, Argentina, are of relatively low thermal conductivities. However, loess covers extensive areas in Asia, Europe and America, for which higher thermal conductivities have been reported (see Table 1). To investigate the effect of higher soil thermal conductivities on thermal exchange capacity of GHEs in loess, numerical models with thermal conductivities of 1·1 and 1·6 W/(m K) have been built and solved and results of 20 years of system operation are shown in Figure 10. The building

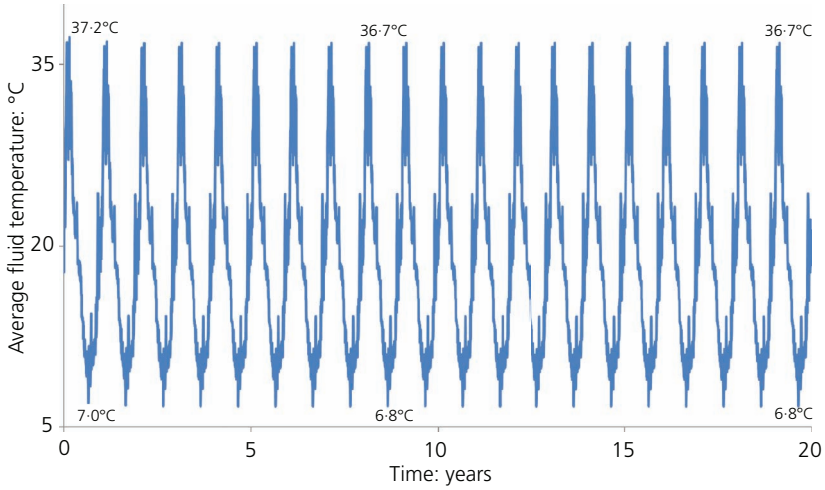

Figure 9. Average GHE fluid temperature in the expanded GHE field during 20 years of operation

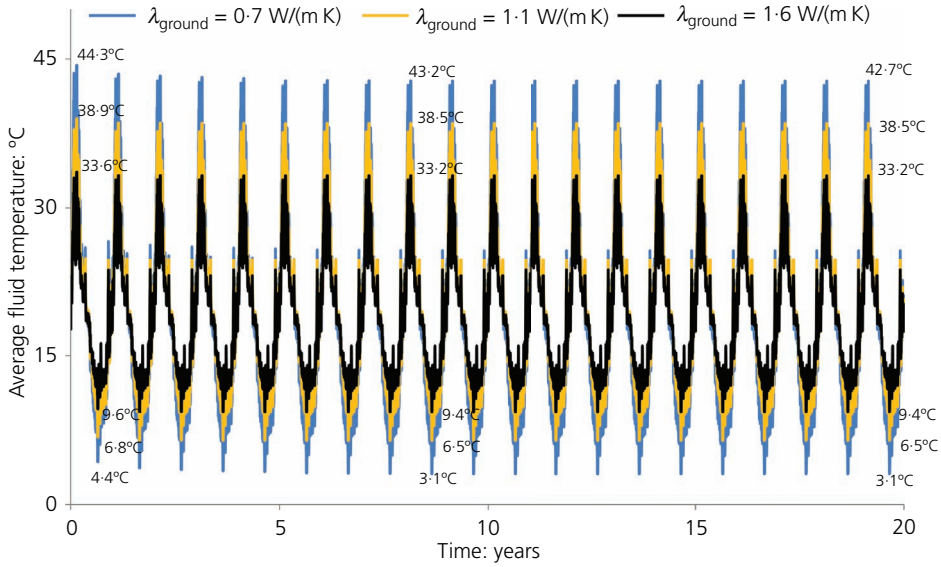

Figure 10. Average GHE fluid temperature during 20 years of operation for higher thermally conductive loessial soils (based on case 1)

thermal load distribution applied on this model follows the pattern shown in Figure 5(a) indicated as case 1, which is applied on 13 9·5 m-long GHEs. It is observed that loessial soil with higher thermal conductivity will significantly improve the thermal performance of GHEs. The maximum fluid temperature in the most thermally affected GHE is about 5·4°C lower than in case 1 when the soil thermal conductivity is equal to 1·1 W/(m K) (38·9°C against 44·3°C). Increasing the thermal conductivity to 1·6 W/(m K), which can be considered as an average value of highly conductive loessial soils based on Table 1, further decreases the maximum fluid temperature to about 33·6°C, which is 10·7°C lower than the maximum fluid temperature observed in case 1. These results suggest that with higher thermal conductivity loess, the GHE field is not working at its full capacity and either the thermal load aimed to be satisfied by the GSHP system can be increased or alternatively the number of additional GHEs can be reduced.

Conclusions

Pile and micropiles in loessial areas can be easily converted into GHEs while being built. Results from realistic detailed modelling show that the partial substitution of electrical heating

and cooling systems with geothermal systems consisting of 13 energy piles could significantly reduce energy consumption and the size of associated infrastructure (electricity grid). The temperate climate dominating in Córdoba presents ideal conditions for GSHP systems, allowing thermal recharge of the ground between seasons and thus maximizing the heating and cooling capacity that energy piles can achieve; similar conditions apply to other parts of the world. Results shows that the 13 energy piles embedded under the residential case study building are capable of delivering approximately 54% and 33% of the heating and cooling demand of the building, respectively. The addition of 12 extra GHEs to the GHE field allows satisfying 100% of the heating demand and 60% of the cooling demand. Consequently, additional savings are achieved on the energy bills (running costs) and on the (smaller) auxiliary systems still needed to cover the remaining 40% cooling demand (capital costs). This case study shows the potential of GSHP technology in a local environment dominated by loess and gives some bases to geotechnical engineers to start considering the technology in their designs and practices.

A parametric analysis of thermal conductivity of loessial soil confirms that the higher thermal conductivity of the soil significantly helps to reduce the number of GHEs in the system. As the loessial soils around the world show thermal conductivities varying between 0·1 and about 2 W/(m K), numerical results suggest that GSHP systems in loessial soils of higher thermal conductivity (e.g. Europe and Asia) show a great potential to economically satisfy conditioning of buildings and encourages further application of this technology in loessial soils.

Acknowledgements

Funding from Australian Research Council (ARC) FT140100227 and the University of Melbourne is much appreciated. The authors would also like to acknowledge the contributions of H. Ferrero (Profundar), C. Serrano (GEoS and UCC) and E. Delacoste (UNC) regarding information about the residential case study and loess thermal properties.

REFERENCES

Amatya B, Soga K, Bourne-Webb P and Laloui L (2012) Thermo-mechanical performance of energy piles. *Geotechnique* **62(6)**: 503–519.

ASTM (2008) D 5334: Standard test method for determination of thermal conductivity of soil and soft rock by thermal needle probe procedure. ASTM International, West Conshohocken, PA, USA.

Baggs S, Baggs D and Baggs JC (1991) *Australian Earth-Covered Buildings*. New South Wales University Press, Kensington, Australia.

Barnard A, Hunt W, Timlake W and Varley E (1966) A theory of fluid flow in compliant tubes. *Biophysical Journal* **6(6)**: 717–724.

Bidarmaghz A (2014) *3D Numerical Modelling of Vertical Ground Heat Exchangers*. PhD thesis, The University of Melbourne, Australia.

Bidarmaghz A, Narsilio G, Johnston I and Colls S (2016) The importance of surface air temperature fluctuations on long-term performance of vertical ground heat exchangers. *Geomechanics for Energy and the Environment* (under review).

Brandl H (2006) Energy foundations and other thermo-active ground structures. *Geotechnique* **56(2)**: 81–122.

Dec D, Dörner J and Horn R (2009) Effect of soil management on their thermal properties. *Revista de la Ciencia del Suelo y Nutrición Vegetal* **9(1)**: 26–39.

Francisca FM (2007) Evaluating the constrained modulus and collapsibility of loess from standard penetration test. *International Journal of Geomechanics* **7(4)**: 307–310.

Gogół W, Gogół E and Artecka E (1973) Thermal conductivity investigations of moist soils. *Journal of Power Technologies* **40**: 49–69.

Guan X, Huang J, Guo N, Bi J and Wang G (2009) Variability of soil moisture and its relationship with surface albedo and soil thermal parameters over the Loess Plateau. *Advances in Atmospheric Sciences* **26(4)**: 692–700.

Günster N, Eck P, Skowronek A and Zöller L (2001) Late Pleistocene loess and their paleosols in the Granada Basin, Southern Spain. *Quaternary International* **76–77**: 241–245.

He K, Wang B and Zhang G (2000) Study on soil thermal properties in forest land of catchment in loess. *Journal of Beijing Forestry University* **22(3)**: 27–32.

Iriondo MH (1997) Models of deposition of loess and loessoids in the Upper Quaternary of South America. *Journal of South American Earth Sciences* **10(1)**: 71–79.

Johnson JB and Lorenz RD (2000) Thermophysical properties of Alaskan loess: an analog material for the Martian polar layered terrain. *Geophysical Research Letters* **27(17)**: 2769–2772.

Johnston I, Narsilio G and Colls S (2011) Emerging geothermal energy technologies. *KSCE Journal of Civil Engineering* **15(4)**: 643–653.

Kodešová R, Vlasakova M, Fer M *et al.* (2013) Thermal properties of representative soils of the Czech Republic. *Soil and Water Research* **8(4)**: 141–150.

Kostić N and Protić N (2000) Pedology and mineralogy of loess profiles at Kapela-Batajnica and Stalać, Serbia. *Catena* **41(1)**: 217–227.

Kröhling DM and Iriondo MN (1999) Upper Quaternary palaeoclimates of the Mar Chiquita area, North Pampa, Argentina. *Quaternary International* **57–58**: 149–163.

Kukla G and An Z (1989) Loess stratigraphy in central China. *Palaeogeography, Palaeoclimatology, Palaeoecology* **72(3–4)**: 203–225.

Leighton MM and Willman HB (1950) Loess formations of the Mississippi Valley. *The Journal of Geology* **58(6)**: 599–623.

Little EC, Lian OB, Velichko A *et al.* (2002) Quaternary stratigraphy and optical dating of loess from the east European plain (Russia). *Quaternary Science Reviews* **21(14)**: 1745–1762.

Loveridge F and Powrie W (2014) 2D thermal resistance of pile heat exchangers. *Geothermics* **50**: 122–135.

Lurie MV (2008) *Modeling and Calculation of Stationary Operating Regimes of Oil and Gas Pipelines*. Wiley, Weinheim, Germany.

Marschalko M, Yilmaz I, Fojtova L, Lamich D and Bednarik M (2013) Properties of the loess sediments in Ostrava region (Czech Republic) and comparison with some other loess sediments. *The Scientific World Journal* **2013**, Article ID 529431.

Moll L and Rocca R (1991) Properties of loess in the center of Argentina. In *XI Pan American Conference on Soil Mechanics and Foundation Engineering*. Viña del Mar, Chile, pp. 1–14.

Narsilio G, Francisca F, Ferrero H *et al.* (2015) Geothermal energy in loess: a detailed numerical case study for Cordoba. *XV Panamerican Conference on Soil Mechanics and Geotechnical Engineering.* Buenos Aires, Argentina.

Oklahoma State University (2009) *Ground Source Heat Pump Residential and Light Commercial Design and Installation Guide*. International Ground Source Heat Pump Association, Stillwater, OK, USA.

Preene M and Powrie W (2009) Ground energy systems: from analysis to geotechnical design. *Geotechnique* **59(3)**: 261–271.

Quintana Crespo E (2005) *Relación entre las Propiedades Geotécnicas y los Componentes Puzolánicos de los Sedimentos Pampeanos*. PhD thesis, Universidad Nacional de Córdoba, Córdoba, Argentina (in Spanish).

Rinaldi V, Rocca R and Zeballos M (2007) *Geotechnical Characterization and Behavior of Argentinean Collapsible Loess*. Taylor & Francis, Boca Raton, FL, USA.

Rocca R (1985) *Review of Engineering Properties of Loess*. MSc thesis, University of California, Berkeley, CA, USA.

Rocca RJ, Redolfi ER and Terzariol RE (2006) Características geotécnicas de los loess de Argentina. *Revista Internacional de Desastres Naturales, Accidentes e Infraestructura Civil* **6(2)**: 149–166 (in Spanish).

Teruggi ME (1957) The nature and origin of Argentine loess. *Journal of Sedimentary Research* **27(3)**: 322–332.

Terzariol RE (2009) Años de estudio de los suelos loessicos en Córdoba, Argentina. *Desafíos y Avances de la Geotecnia Joven en Sudamérica* **1**: 323–337 (in Spanish).

Usowicz B, Kossowski J and Baranowski P (1996) Spatial variability of soil thermal properties in cultivated fields. *Soil and Tillage Research* **39(1)**: 85–100.

Wang TH, Liu ZC and Lu J (2007) Experimental study on coefficient of thermal conductivity and specific volume heat of loess. *Yantu Lixue (Rock and Soil Mechanics)* **28(4)**: 655–658.

Zárate MA (2003) Loess of southern South America. *Quaternary Science Reviews* **22(18)**: 1987–2006.

Zuo J, Wang J, Huang J *et al.* (2011) Estimation of ground heat flux and its impact on the surface energy budget for a semi-arid grassland. *Sciences in Cold and Arid Regions* **3(1)**: 41–50.